

Characterisation of single cell response to shock waves and *in silico* optimisation of shock wave-mediated therapy

D. Li, A. Pellegrino, A. Hallack, N. Petrinic, A. Jérusalem, and R. Cleveland

(Dated: September 5, 2017)

Abstract

Shock waves have been used in several medical treatments including lithotripsy and orthotripsy and suggested for cancer therapy. The therapeutic efficacy of shock wave-mediated treatments is mainly limited by the trade-off between therapeutic outcome and side-effects. In order to advance the use of shock waves for treatments, the interaction between shock waves and cells needs to be understood. Here, ultra-high speed imaging was used to visualise single cell deformation under shock wave exposure in a tissue-mimicking phantom with HRE, HK-2 and CAKI-2 cell lines. The experimental results showed a small cell area decrease ($<2\%$) during the compressive phase of the shock wave but a large cell area expansion ($\sim 10\%$) during the tensile phase, indicating different cell behaviours under the compressive and tensile loading. In addition, this result along with the cell viability test indicates a difference in cell response to shock waves for different cell types (cancerous vs. non-cancerous).

The experimental observations, of cell deformation under shock waves, were captured by a numerical model with a constitutive material framework consisting of an Equation of State for the volumetric response and hyper-viscoelasticity for the deviatoric response. The volumetric cell response was modelled with two different bulk moduli for the compressive and tensile shock loading.

Three kidney epithelial cell lines representing cancer cells, normal healthy cells and virus-transformed cells were studied. It was discovered that cancer cells showed a smaller deformation but with faster response to the shock wave tensile phase compared to their non-cancerous counterparts, providing insights into shock wave-mediated therapeutic drug delivery and cancer cell rupture. For a shock wave with a tensile stress of 4.59 MPa, the model predicts increased cell membrane permeability on target cancer cells with minimal interference on normal cells.

I. INTRODUCTION

A shock wave is a type of acoustic wave characterised by the presence of a rapid pressure jump governed by the interaction of non-linear effects which steepen the waveform and attenuation mechanisms which smooth the waveform [1]. Shock waves have been medically used for decades in a procedure called lithotripsy in which shock waves fragment kidney stones. Although lithotripsy is a mature technology, there are concerns about bioeffects including renal haemorrhage and scarring with a permanent loss of functional renal volume [2, 3]. This motivates a better understanding of shock wave interaction with tissue in order to reduce side-effects. Although damage is predominantly thought to be induced by cavitation [4, 5], even in environments where cavitation is minimised, damage has been reported in cells [6] and tissues [7], suggesting a direct impact of shock waves on cells.

Shock waves have also been employed for orthotripsy, the treatment of musculoskeletal disorders such as plantar fasciitis, tendon pain and non-unions or delayed unions of long bone fractures [8]. The mechanism by which shock waves have an effect on musculoskeletal conditions is not understood. One of the hypotheses is that the disruption of the tissue by shock waves results in “microtrauma” which then induces neovascularisation believed to improve blood supply and tissue regeneration. The increased permeability of the vessel wall may also promote the healing process [8].

Cancer therapy is another field in which shock waves have been investigated [9–11]. It has been reported that besides mechanically rupturing cells, shock waves may enhance the sonoporation effect which temporarily increases the membrane permeability to allow molecules in the surrounding medium to diffuse into cells [9]. This provides a mechanism for shock wave-mediated therapeutic drug delivery and gene transfer. Furthermore, some experimental results have shown a positive influence of shock waves on suppressing tumour growth and selectively killing malignant cells [10, 11]. The mechanisms by which shock waves affect cancer cells are not well understood.

The goal of this work is to develop a numerical model for studying single cell response to shock waves, calibrated and validated against ultra-high speed imaging of single cell deformation under the action of shock waves. The difference in cell response to shock waves due to cell types is also examined. The numerical model employs a 3D continuum model of an individual cell modelled with a combined Equation of State (EoS) and hyper-

viscoelastic material framework. The validated numerical model was then used to analyse the development of the stress and strain fields under the compressive and tensile phases of the shock wave, from which insights into the mechanisms of cell destruction and sonoporation were obtained. Two shock wave profiles are proposed to specifically target cancer cells for enhanced sonoporation or rupture while minimising impact on normal healthy cells.

II. EXPERIMENTAL STUDY

The experimental rig consisted of a shock wave source coupled to a tissue-mimicking gel in which cells were embedded. The gel contained cell media in order to maintain cell viability. Three kidney epithelial cell lines representing cancer cells, normal healthy cells and virus-transformed cells were studied. An ultra-high speed camera (SIMX 16, Specialised Imaging) with $20\times$ objective (UMPLFLN20XW, Olympus) was used to image individual cells. Prior to the cell experiments the camera and shock source were co-aligned with a needle hydrophone.

For each experiment, the camera was focussed onto a cell in the focal region of the shock waves. A reference image was taken before the delivery of shock waves. A shock wave was delivered and the camera was triggered to capture 16 frames at a rate of 3.3 Mfps (interframe time of 300 ns with an exposure time of 200 ns). Each cell was imaged with three different shock wave energy settings. The imaging experiment was repeated on eight different target cells for each of the three cell lines investigated. Further details of the experimental system are described in the SI.

The high speed images were filtered and then processed to extract the boundary of the cells from the images using methods described in the SI. The deformation of the cell was determined by comparing the cell boundary during shock wave passage to the cell boundary in the reference image; we note that a separate reference image was used for each camera channel to avoid channel-to-channel differences. Quantitative analysis of the perimeter and area change was performed based on the extracted cell boundaries.

Shock wave pressure profiles. Fig. 1 shows pressure waveforms measured at the focus of a clinical shock wave source (Minilith SL1-0G, STORZ) at three different energy settings (levels 4, 6 and 8), using a bespoke fibre-optic probe hydrophone embedded in a tissue-mimicking phantom [12]. In each case the shock wave consists of a compressive

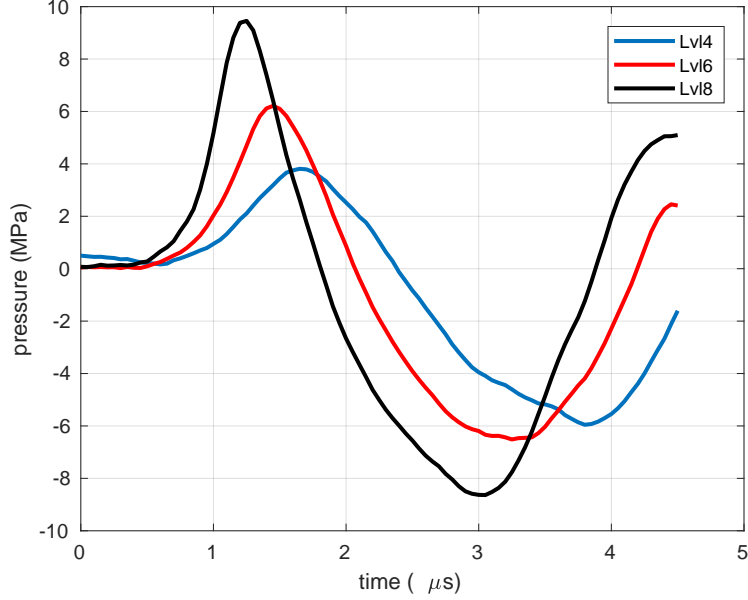


FIG. 1: Measured focal shock waves in a tissue-mimicking phantom for source energy level 4 (blue), level 6 (red) and level 8 (black).

phase (duration around $1.5 \mu\text{s}$) followed by a tensile phase (duration around $2.1 \mu\text{s}$). As the energy level increased three effects were observed: an increase in the peak positive pressure; a decrease in the shock rise time (time duration for the shock front pressure to rise from 10% to 90% of the maximum shock pressure); and a gradual increase in the peak negative pressure. These are characteristic behaviours of a focussed non-linear acoustic wave [13].

Single cell deformation under a shock wave. Fig. 2(a)-(c) show representative images of an individual healthy human kidney (HRE, Lonza) cell during the compressive phase of a shock wave at energy level 8. The cell boundary was extracted, as described in the SI, and it can be seen that the cell is translated and the contour is slightly compressed in this phase of the shock wave. Fig. 2(d)-(f) show the cell during the tensile phase and it can be seen that the boundary has expanded and also become more diffuse in the image. As described in the SI the effects of variability in the imaging, segmentation and acousto-optic interactions were analysed, and were found not to mask the cell deformation under shock waves.

The projected cell area inside the cell boundary was calculated for every image and Fig. 3(a)(d)(g) show the area change-time curve for HRE cells for the three shock wave energy settings. It can be seen that the cells initially undergo a small compression ($<2\%$ area decrease) followed by a large expansion which increases with the increase of shock wave energy

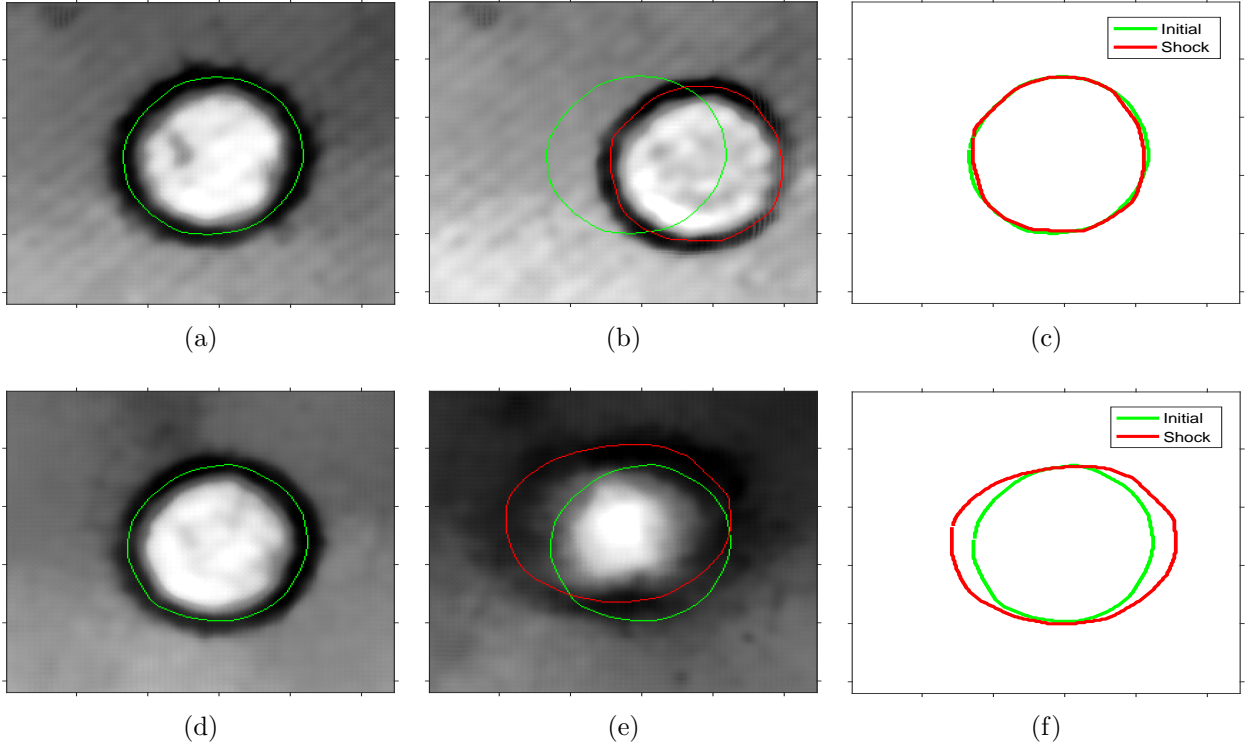


FIG. 2: Deformation of a healthy HRE cell during the compression phase ((a)-(c)) and tension phase ((d)-(f)) at energy level 8: (a)(d) before shock wave (b)(e) during shock wave interaction (c) cell contour comparison before (green) and during (red) shock wave exposure.

levels (up to 13% area increase at shock wave energy level 8). The timing of cell deformation was found to be consistent with the compressive phase and tensile phase of the shock wave, however, the six-fold increase in cell area changes between tension and compression was not consistent with the fact that the magnitude of tensile stress was comparable to that of compression with similar loading rates. These data suggest that the cells are stiffer during compression than under tension.

The experiments were repeated with virus-transformed immortalised kidney cells, HK-2 (Fig. 3(b)(e)(h)), and kidney cancer cells, CAKI-2 (Fig. 3(c)(f)(i)). Both the cancer cells and immortalised cells exhibit the same qualitative behaviour as the healthy cells (a small response to the compressive phase and large response to the tensile phase of the shock wave). Further the cell area change increases with the shock wave energy level setting and the difference in the maximum area increase among the three cell types also becomes more distinguishable, see SI. At energy level 8, the maximum area increase was 13% in HRE (Fig. 3(g)), 17% in the HK-2 cells (Fig. 3(h)) and 9% in CAKI-2 (Fig. 3(i)). The difference was

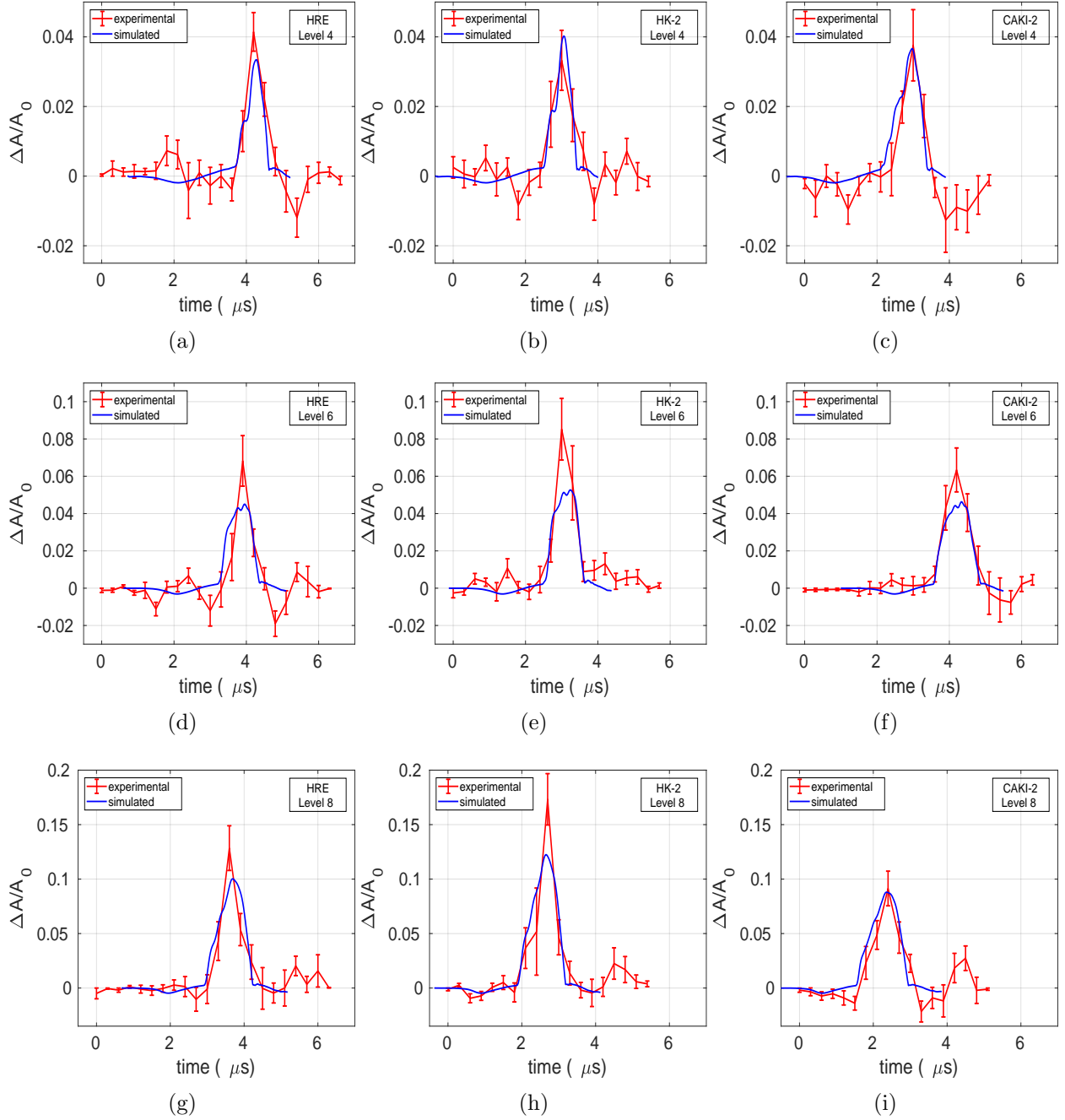


FIG. 3: Experimental (red) and simulation (blue) results of cell area change in response to shock waves. The cell deformation at shock wave energy levels: (a)-(c) level 4, (d)-(f) level 6, (g)-(i) level 8 for HRE (a)(d)(g), HK-2 (b)(e)(h) and CAKI-2 cells (c)(f)(i). The error bar shows the standard error based on 9 individual cells for each case.

statistically significant for HK-2 and CAKI-2 cells with a p-value of less than 0.05 in the Mann-Whitney U test. Furthermore, the duration of cell area expansion was longer for the CAKI-2 cells ($\sim 1.8 \mu s$) than for the HRE and HK-2 cells ($\sim 1.5 \mu s$). These results indicate

that the CAKI-2 cells exhibit stiffer mechanical characteristics during tension than normal or virus-transformed cells. We note that the duration of the tensile deformation of cells was slightly shorter than the 2.1 μ s duration of the shock wave tensile phase which suggests there may be a hysteresis effect presented in the transition from compression to expansion.

The projected cell area can be thought as a proxy for the volumetric deformation of the cell and the cell perimeter for assessing its deviatoric response. It was found that the ratio of the projected area change to perimeter change for all three cell types at the three different energy level settings remained between 1.5 and 2, which results in less than a 10% variation from a circular shape (analysis presented in the SI) and therefore suggests that the cells did not undergo substantial shear deformation during the shock wave exposure. A measure of shear related perimeter change was calculated by factoring out the volumetric contribution. It was found that the shear-related perimeter change for all three cell types remain less than 0.5%, further suggesting a small shearing effect in the experiment. More details are provided in the SI.

Cell viability test. In order to investigate the difference in cell response to shock waves for different cell types embedded in the agarose gel, a cell viability test was performed using a lactate dehydrogenase (LDH) assay after shock wave exposure. Cell viability is determined by light absorbance and in order to measure a detectable signal, $\sim 500,000$ cells were concentrated to the shock wave focal zone and exposed to 500 shock waves at energy levels 4 and 8. The detailed experimental protocol is explained in the SI.

Fig. 4 shows the results of cell cytotoxicity after shock wave exposure at energy levels 4 and 8. It can be seen that at energy level 4 no shock wave induced cytotoxicity was observed. The negative values indicate that shock wave treated cell samples presented higher cell viability than the non-treated sham samples. This effect has been found in previous studies where lower amplitude shock waves enhanced cell proliferation [14, 15]. At energy level 8 all three cell lines exhibited cell cytotoxicity after shock wave exposure; and the cancer cell line (CAKI-2) suffered higher cytotoxicity compared to the other two normal cell lines (HK-2 and HRE).

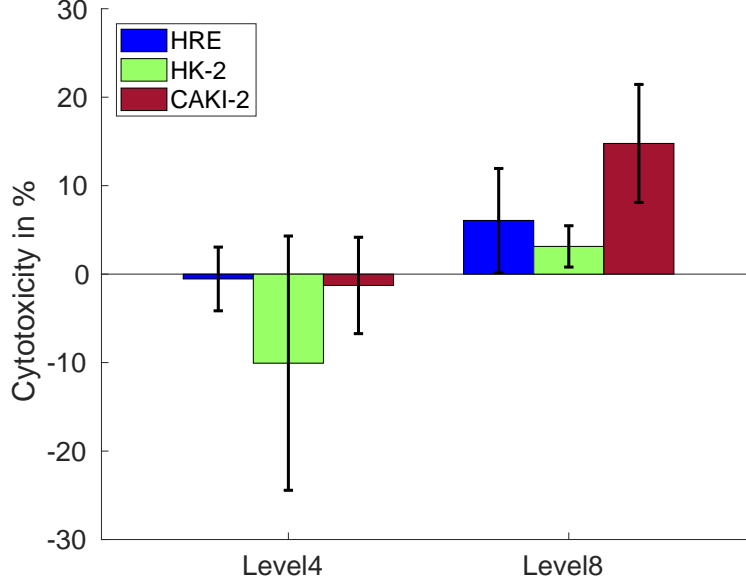


FIG. 4: Cell cytotoxicity of different cell lines at shock wave energy levels 4 and 8. The error bar represents the standard deviation calculated from 6 experimental repeats for each cell line and shock wave condition. Welch's ttests showed a statistically significant difference between CAKI-2 and HK-2 or HRE ($p < 0.05$).

III. NUMERICAL STUDY

The 3D finite element model employed here consisted of a cell surrounded by extracellular matrix. The deformation was decomposed into a deviatoric response and a volumetric response. The deviatoric response was described by the first order generalised Maxwell viscoelasticity, which consists of a long term shear modulus (μ_∞), a viscous shear modulus (μ_i) and a viscosity (η_i) [16]. The volumetric response was modelled by a bilinear acoustic EoS which employed different bulk moduli for the compressive and tensile phases of the shock wave. The surrounding matrix was modelled by non-linear elasticity in combination with an acoustic EoS.

The measured shock waves (see Fig. 1) were used as boundary conditions for the top surface of the model and propagated as a plane wave through the computational domain. Further details are presented in the SI.

Numerical model calibration and validation. The mechanical properties of the numerical model under ultra-high strain rate loading were calibrated against the experimental measurement of the cell area change.

Based on the larger deformation observed in the tensile phase than in the compressive

phase, a bilinear EoS was proposed to model the volumetric change of a single cell subject to shock waves. This EoS employs a high bulk modulus in compression and a lower bulk modulus in tension with a transition pressure threshold to govern the transition between them. The compressive bulk modulus was estimated to be 2 GPa due to the small cell deformation under compression as well as the water content of the cell (pure water has a bulk modulus of 2.2 GPa [17]). The other two material parameters (i.e., tensile bulk modulus and transition pressure threshold) were calibrated for each cell line by minimising the least square error of cell area change between the simulation and experimental results.

The final mechanical properties of the model calibrated across all three shock wave energy levels are presented in Table I.

TABLE I: Mechanical properties for different cell types

	compressive bulk modulus	tensile bulk modulus	transition pressure
CAKI-2	2 GPa	34 MPa	-4 MPa
HK-2	2 GPa	20 MPa	-4.6 MPa
HRE	2 GPa	25 MPa	-4.6 MPa

The bulk moduli and transition pressure for HK-2 and HRE cells are similar while the CAKI-2 cells exhibit a higher modulus in tension and a lower transition pressure. The mechanical properties suggest that even though the cancer cells have the largest bulk modulus, the lower transition pressure threshold make them the first to undergo large deformation during tension.

The simulation results of the cross-sectional area change (which is equivalent to the projected cell area from the experiments) for each cell line using the optimised material parameters are presented in blue in Fig. 3. It can be seen that the simulations capture the response across all three energy levels with one unique set of material properties for each cell line. During the calibration process the influence of the deviatoric material properties (shear moduli and viscosity) on the cell area change was found to be insignificant (a factor of 10^6 in the deviatoric properties resulted in $<0.01\%$ of area change). This is consistent with the experimental observations that the cell response is dominated by its volumetric deformation. The deviatoric properties used in the study were obtained from literature ($\mu_0 = 3.1$ kPa, $\mu_1 = 0.34$ kPa, $\eta = 69.6$ Pa.s) [18, 19].

Quantification of stress and strain evolution of cells. The numerical model quan-

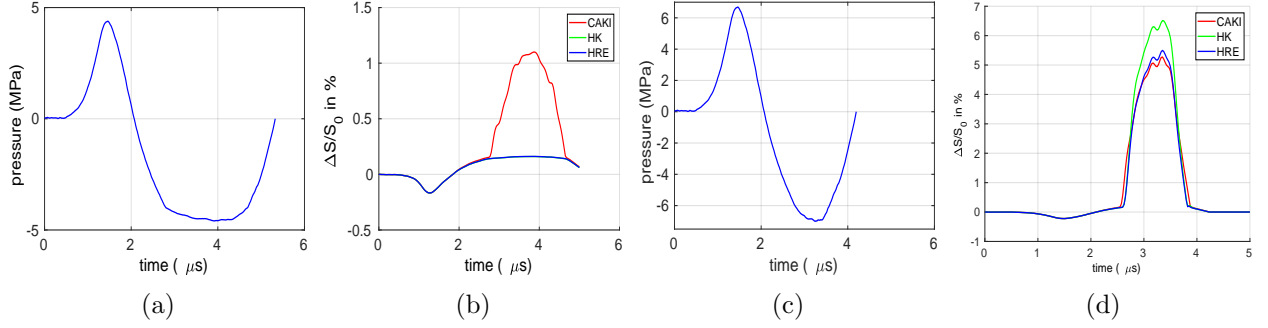


FIG. 5: (a) First proposed shock loading with a maximum tensile pressure of 4.59 MPa; (b) resultant cell membrane strain in three cell types; (c) second proposed shock loading with a maximum tensile pressure of 7 MPa; (d) resultant cell membrane strain in three cell types.

tifies the cell response in terms of stress and strain evolutions in 3D which provides insights into shock wave interactions with cells. The shock wave propagation was found to be not strongly influenced by the difference in mechanical properties between the cell types. The von Mises stress quantifying the amount of shearing in the model, was found to be of the order of 100 Pa using the deviatoric mechanical properties from the literature. The overall cell membrane strain, which describes the area change of the cell membrane, was also analysed as an indicator of cell membrane permeability showing the maximum values of 10% in HRE, 12% in HK-2 and 8.5% in CAKI-2 cells at shock wave energy level 8. More details are provided in the SI.

Optimisation of shock wave loading. The validated numerical model allows for testing of designed shock wave profiles to elicit a specific cell response. For example, a shock wave with a tensile stress of the order of 4.5 MPa will exceed the transition threshold of cancer cells but not healthy cells, and therefore could sonoporate or even rupture cancer cells without damaging normal cells. Fig. 5(a)(b) present a proposed shock wave profile with a peak negative pressure of 4.59 MPa and the predicted membrane strain for each cell type. The difference in the threshold for CAKI-2 and HRE (HK-2) cells resulted in a 1.1% of membrane strain in CAKI-2 cells at the maximum tensile pressure while that of HK-2 and HRE cells remained less than 0.2%. The rupture strain threshold for cancer cells have been reported to be around 5% [20, 21], therefore with 1.1% of tensile membrane strain, increased cell membrane permeability may be expected even though permanent damage may not occur.

Research studies have also shown that the rupture strain threshold is 40% or higher for

normal cells [22, 23]. Therefore another shock loading with the peak negative pressure of 7 MPa was proposed, see Fig. 5(c), which is expected to result in rupture of cancer cells ($>5\%$ membrane area increase). In this case, the non-cancerous cells (HK-2 and HRE cells) showed relatively large deformation during tension ($\sim 5.5\%$ and 6.5% respectively) which, however, are still well below the reported rupture threshold for normal cells. In addition the expansion in cancer cell was longer in duration compared to their non-cancerous counterparts (HK-2 and HRE cells), which may lead to higher energy deposition for damaging cancer cells.

IV. DISCUSSION

The key result in this work is that cells subject to shock waves were stiffer under compression (compressive deformation $<2\%$) than under tension (tensile deformation $\sim 10\%$) even though the compressive phase of the shock wave was comparable to that in the tensile phase. This phenomenon was captured in the simulation by using a bilinear model for the bulk modulus in the EoS: with a high modulus for compression and lower modulus for tension with a transition pressure threshold.

Differences in cell deformation under compression and tension have been reported at lower strain rates and are related to the cytoskeletal network which consists of actin filaments, intermediate filaments and microtubules, bathed in a fluid environment (the cytosol) [24]. It has been suggested that actin filaments and intermediate filaments provide resistance to tension (acting like springs) while microtubules are resistant to compression (acting like rods) [25]. It is thus expected that cells behave differently under different external loading (e.g., compression versus tension). Furthermore, the observed cell deformation is also consistent with the concept that under compression the presence of water in the cells results in a bulk modulus similar to water. Under tension the decrease in bulk modulus beyond a critical tensile stress suggests that some combination of mechanical structure failure and fluid cavitation may be at play within the cell. However, in the data shown in Fig. 3 no macroscopic failure or cavitation was directly observed. Possible mechanisms for micro-rupture include: intracellular cavitation in the cytoplasm [26], intramembrane cavitation where rupture occurs between the layers of the lipids that make up the cell membrane [27], or phase transition of the lipids in the cell membrane from a gel state to a fluid state [28]. The presence of large deformation under tension indicates that both cell damage and increased

membrane permeability are likely to occur during this stage of the shock loading.

Fitting of the numerical models to the measured cell deformation suggested that CAKI-2 cells have a greater tensile stiffness than HK-2 and HRE cells. This contrasts with the general consensus that cancers cells have lower stiffness than normal cells [29, 30], although there are also reports of cancer cells having greater stiffness than normal cells [31, 32]. Additionally, previously reported stiffness values refer to the Young's modulus measured at slow strain rates ($<10 \text{ s}^{-1}$), while we report the bulk modulus at very high strain rate ($>10^4 \text{ s}^{-1}$), at which a strong strain rate effect is expected. Note also that the bulk modulus and Young's modulus will not be strongly correlated, particularly when the Poisson's ratio is close to 0.5 as is expected for cells.

The cell viability experiments indicate that shock waves at energy level 4 did not result in cell death for any of the cell types. The simulations predicted that the maximum tensile membrane strains of both cancerous and normal healthy cell lines at energy level 4 are less than 4% (Fig. 19(a), SI). Previous work has reported that the rupture strain threshold for cancer cells is around 5% [20, 21] while that of normal cells have been reported to be 40% or higher [22, 23]. The predicted strains induced by energy level 4 are less than these values (with the caveat that these reports are at low strain rates) and therefore the lack of cell death is consistent with the strains being below the damage threshold. For the experiments at energy level 8 CAKI-2 cells exhibited greater cell toxicity than normal cells; this was despite the fact that the larger bulk modulus of the cancerous cells meant that the simulations predicted that the CAKI-2 cells should experience a peak tensile membrane strain (8%, Fig. 19(c), SI) smaller than that of normal cells ($>10\%$, Fig. 19(a), SI). The difference is consistent with the reports that cancerous cells are more fragile than normal cells; and that this effect is more important than the change in the bulk modulus.

These results motivated the design of shock wave profiles to specifically target cancer cells for therapy without affecting normal cells. The first was designed to facilitate sonoporation into cancer cells by employing a shock wave with a peak tensile pressure of -4.59 MPa which should exceed the transition pressure threshold of cancer cells (-4 MPa) but not that of normal cells (-4.6 MPa). Results from the simulations, depicted in Fig. 5(a)(b), predicted a 1.1% membrane strain increase for CAKI-2 cells as opposed to 0.2% found for the HK-2 and HRE cells. The strain in the CAKI-2 cells should be sufficient to result in cell membrane permeability, without inducing cell death, while having no effect on healthy cells. The

second designed shock wave profile employed a higher tensile pressure and resulted in $>5\%$ membrane strain in cancer cells (Fig. 5(c)(d)) for cancer cell rupture while the predicted membrane stretch was of $\sim 5\%$ in normal cells; these strains should result in cell death for CAKI-2 cells (which are more fragile) while leaving normal cells intact.

We acknowledge that the experimental setup employed here does not fully capture *in vivo* conditions. Embedding cells in transparent gel allowed for the visualisation and study of single cell deformation under shock waves in the presence of a scaffold that captures the bulk mechanical properties of tissue. Ideally the cells under investigation would be in contact with surroundings; however this setup is crucial to study cell behaviour at cellular or subcellular level (e.g., therapeutic molecules permeate cell membranes).

In conclusion, this work reports the first quantitative combination of experimental measurements and numerical simulations of the deformation of single cells in response to shock waves. The experimental results showed that dominant response of the cells was during the tensile phase of the shock waves with a tensile strain of $\sim 10\%$ for a peak tensile pressure around -8 MPa. A bilinear bulk modulus with tensile yield stress was used to capture the observed asymmetry between compression and tension. The experiments and simulations suggest that cell damage or sonoporation effects occur during the tensile phase, even though the pressure magnitude is greater in compression. The numerical model was then used to identify shock wave profiles that can differentiate the tensile responses between cancer cells and non-cancerous cells in order to achieve cancer cell-specific therapy: sonoporation and cell damage.

-
- [1] R. O. Cleveland and J.A. McAteer. *The Physics of Shock-Wave Lithotripsy*, volume 1, chapter 49, pages 529–558. Smith's Textbook of Endourology 3rd Edition, 2012.
 - [2] Jonathan Silberstein, Charles M Lakin, and J Kellogg Parsons. Shock wave lithotripsy and renal hemorrhage. *Reviews in Urology*, 10(3):236, 2008.
 - [3] James A McAteer and Andrew P Evan. The acute and long-term adverse effects of shock wave lithotripsy. In *Seminars in nephrology*, volume 28, pages 200–213, 2008.
 - [4] Edwin L Carstensen, Sheryl Gracewski, and Diane Dalecki. The search for cavitation in vivo. *Ultrasound in Medicine & Biology*, 26(9):1377 – 1385, 2000.

- [5] Brian R Matlaga, James a McAteer, Bret a Connors, Rajash K Handa, Andrew P Evan, James C Williams, James E Lingeman, and Lynn R Willis. Potential for cavitation-mediated tissue damage in shockwave lithotripsy. *Journal of endourology / Endourological Society*, 22(1):121–6, 2008.
- [6] James C Williams Jr, Jason F Woodward, Mark A Stonehill, Andrew P Evan, and James A McAteer. Cell damage by lithotripter shock waves at high pressure to preclude cavitation. *Ultrasound in medicine & biology*, 25(9):1445–1449, 1999.
- [7] Andrew P Evan, Lynn R Willis, James a McAteer, Michael R Bailey, Bret a Connors, Youzhi Shao, James E Lingeman, James C Williams, Naomi S Fineberg, and Lawrence a Crum. Kidney damage and renal functional changes are minimized by waveform control that suppresses cavitation in shock wave lithotripsy. *The Journal of urology*, 168(4 Pt 1):1556–1562, oct 2002.
- [8] Ching Jen Wang. An overview of shock wave therapy in musculoskeletal disorders. *Chang Gung medical journal*, 26(4):220–232, 2003.
- [9] R Murata, K Nakagawa, S Ohtori, N Ochiai, and H Moriya. The effects of radial shock waves on gene transfer in rabbit chondrocytes in vitro. 15(11):1275–1282, 2007.
- [10] F Gamarra, F Spelsberg, M Dellian, and A E Goetz. Complete local tumor remission after therapy with extra-corporeally applied high-energy shock waves (HESW). *International journal of cancer. Journal international du cancer*, 55(1):153–6, 1993.
- [11] Martin Oliver Steinhauser and Mischa Schmidt. Destruction of cancer cells by laser-induced shock waves: recent developments in experimental treatments and multiscale computer simulations. *Soft matter*, 10(27):4778–88, 2014.
- [12] JE. Parsons, CA. Cain, and J Brian Fowlkes. Cost-effective assembly of a basic fiber-optic hydrophone for measurement of high-amplitude therapeutic ultrasound fields. *The Journal of the Acoustical Society of America*, 119(3):1432–40, 2006.
- [13] MA Averkiou and MF. Hamilton. Nonlinear distortion of short pulses radiated by plane and focused circular pistons. *The Journal of the Acoustical Society of America*, 102(5 Pt 1): 2539–48, 1997.
- [14] Sandra Nwokeoha, Robert Carlisle, and Robin O. Cleveland. The Application of Clinical Lithotripter Shock Waves to RNA Nucleotide Delivery to Cells. *Ultrasound in Medicine and Biology*, 42(10):2478–2492, 2016.
- [15] Anna M. Weihs, Christiane Fuchs, Andreas H. Teuschl, Joachim Hartinger, Paul Slezak,

- Rainer Mittermayr, Heinz Redl, Wolfgang G. Junger, Harald H. Sitte, and Dominik Rünzler. Shock wave treatment enhances cell proliferation and improves wound healing by ATP release-coupled Extracellular signal-regulated Kinase (ERK) activation. *Journal of Biological Chemistry*, 289(39):27090–27104, 2014.
- [16] JC Simo and TJR Hughes. *Computational inelasticity*, volume 7. Springer-Verlag New York, 2008.
- [17] C. R. Nave. *Bulk Elastic Properties*. HyperPhysics, 2016.
- [18] Antoine Jérusalem and Ming Dao. Continuum modeling of a neuronal cell under blast loading. *Acta biomaterialia*, 8(9):3360–3371, 2012.
- [19] L M Rebelo, J S De Sousa, J Mendes Filho, and M Radmacher. Comparison of the viscoelastic properties of cells from different kidney cancer phenotypes measured with atomic force microscopy. *Nanotechnology*, 24(5), 2013.
- [20] Leonard Weiss. Biomechanical interactions of cancer cells with the microvasculature during hematogenous metastasis. *Cancer and Metastasis Reviews*, 14(2):187–215, 1992.
- [21] L Weiss, D S Dimitrov, and M Angelova. The hemodynamic destruction of intravascular cancer cells in relation to myocardial metastasis. *PNAS*, 82(17):5737–5741, 1985.
- [22] Fenfang Li, Chon U Chan, and Claus Dieter Ohl. Yield strength of human erythrocyte membranes to impulsive stretching. *Biophysical Journal*, 105(4):872–9, 2013.
- [23] Taiki Shigematsu, Kenichiro Koshiyama, and Shigeo Wada. Effects of stretching speed on mechanical rupture of phospholipid / cholesterol bilayers : Molecular dynamics simulation. *Sci Rep*, 5:15369, 2015.
- [24] Dimitrije Stamenović and Ning Wang. Stress transmission within the cell. *Comprehensive Physiology*, 1(1):499–524, 2011. ISSN 20404603.
- [25] Donald E Ingber. Tensegrity I. Cell structure and hierarchical systems biology. *Journal of cell science*, 116(Pt 7):1157–1173, 2003.
- [26] Emil Brujan. *Cavitation in Non-Newtonian Fluids: With Biomedical and Bioengineering Applications*, volume 7. Springer, 2010.
- [27] Boris Krasovitski, Victor Frenkel, Shy Shoham, and Eitan Kimmel. Intramembrane cavitation as a unifying mechanism for ultrasound-induced bioeffects. *Proceedings of the National Academy of Sciences*, 108, 2011.
- [28] Ruthven N.A.H. Lewis and Ronald N. McElhaney. Membrane lipid phase transitions and phase

- organization studied by fourier transform infrared spectroscopy. *Biochimica et Biophysica Acta (BBA)-Biomembranes*, 10, 2012.
- [29] Q. S. Li, G. Y H Lee, C. N. Ong, and C. T. Lim. AFM indentation study of breast cancer cells. *Biochemical and Biophysical Research Communications*, 374(4):609–613, 2008.
- [30] M Lekka, P Laidler, D Gil, J Lekki, Z Stachura, and a Z Hryniewicz. Elasticity of normal and cancerous human bladder cells studied by scanning force microscopy. *European biophysics journal : EBJ*, 28(4):312–316, 1999.
- [31] Gang Zhang, Mian Long, Zhe-Zhi Wu, and Wei-Qun Yu. Mechanical properties of hepatocellular carcinoma cells. *World Journal of Gastroenterology*, 8(2):243–246, 2002.
- [32] Subra Suresh. Biomechanics and biophysics of cancer cells. *Acta Biomaterialia*, 3(4):413–438, 2007.